ADVANCED QUANTUM TECHNOLOGIES
www.advquantumtech.com

Impact of Parallel Gating on Gate Fidelities in Linear, Square, and Star Arrays of Noisy Flip-Flop Qubits

Marco De Michielis and Elena Ferraro*

Successfully implementing a quantum algorithm involves maintaining a low logical error rate by ensuring the validity of the quantum fault-tolerance theorem. The required number of physical qubits arranged in an array depends on the chosen Quantum Error Correction code and the achievable physical qubit error rate. As the qubit count in the array increases, parallel gating —simultaneously manipulating many qubits— becomes a crucial ingredient for successful computation. In this study, small arrays of a type of donor- and quantum dot-based qubits, known as flip-flop (FF) qubits, are investigated. Simulation results of gate fidelities in linear, square and star arrays of four FF qubits affected by realistic 1/*f* noise are presented to study the effect of parallel gating. The impact of two, three and four parallel one-qubit gates, as well as two parallel two-qubit gates, on fidelity is calculated by comparing different array geometries. The findings can contribute to the optimized manipulation of small FF qubit arrays and the design of larger ones.

1. Introduction

In the realm of semiconductor qubit holders based on donor atoms and quantum dots in silicon,[1–4] the flip-flop (FF) qubit consists of a ^{31}P donor atom situated within a ^{28}Si bulk, positioned at a given distance from the Si/SiO_2 interface. An electric field, generated by a metal gate atop the SiO_2 layer, controls the movement of the donor-bound electron between the donor site and the Si/SiO_2 interface region. By changing the applied electric field the antiparallel electron-nuclear spin states, which defined the FF qubit, can be manipulated. The FF qubit was presented by Tosi et al., in 2017,[5] gained increasing attention in the following years[6–10] and was experimentally demonstrated by Savytskyy et al., in 2023.[11]

FF qubits are of interest due to their exploitation of long-range dipole-dipole interactions,[5] which can mitigate the stringent requirements for precise qubit placement and the resulting inter-qubit spacing.

A reliable assessment of the increase in gate infidelity induced by parallel gating needs to be considered for an accurate estimation of errors in Quantum Error Correction codes, enabling fault-tolerant quantum computation.

When considering array geometry, in addition to the 1D linear array (LA) and the 2D square array (SA), a second 2D array has to be considered: the hexagonal array. At a given inter-qubit distance, the LA is easy to fabricate due to its low qubit density, providing a free area for initialization/readout devices, but it is not suitable for very large arrays unless segmented. The SA is more complex to fabricate due to its higher qubit density and provides less space for initialization/readout devices, but it should be preferred for large arrays due to its 2D geometry. The hexagonal array offers an interesting trade-off, with a lower density than the square one, making it still suitable for large-scale arrays. Hexagonal lattices can be generated by composing replicas of a small star array (STA), where a central qubit is directly coupled with three equidistant qubits placed at the vertices of an equilateral triangle.

The effects of two parallel one- and two-qubit gates applied to four noisy FF qubits arranged in a LA and a SA have been previously studied.[12] Here, we extend this study to include results on a STA and to investigate the effect on fidelity of more than two parallel operations within each array.

2. Model

The Hamiltonian $\hat{H}_A$ describing an array of N FF qubits is:

$$\hat{H}_A = \sum_{i=1}^{N} \hat{H}^i(\Delta E_z^i, E_{ac}^i) + \sum_{i=1}^{N-1} \sum_{j=i+1}^{N} \hat{H}_{int}^{i,j}(\Delta E_z^i, \Delta E_z^j, r_{ij}) \quad (1)$$

where $\hat{H}^i$ is the Hamiltonian of the single FF qubit and $\hat{H}_{int}$ is the dipole-dipole interaction term between qubits i and j.[12] The Hamiltonian $\hat{H}^i$ is a function of a DC electrical field difference $\Delta E_z^i = E_z^i - E_z^0$, where E_z^i is the imposed vertical electric field and E_z^0 represents the vertical electric field at the ionization point, i.e.,

M. De Michielis, E. Ferraro
CNR-IMM
Unit of Agrate Brianza
Via C. Olivetti 2, Agrate Brianza, MB 20864, Italy
E-mail: marco.demichielis@cnr.it

The ORCID identification number(s) for the author(s) of this article can be found under https://doi.org/10.1002/qute.202400341

DOI: 10.1002/qute.202400341

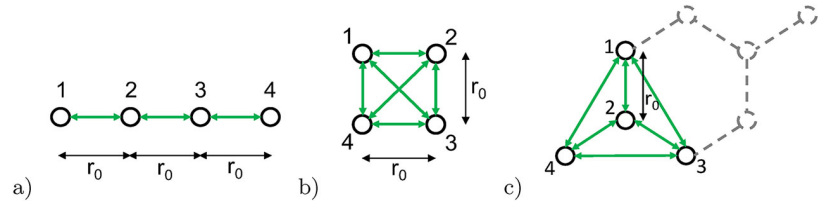

Figure 1. a) LA scheme composed of four FF qubits equally displaced, where r_0 is the inter-qubit distance. Only the first neighbor inter-qubit interactions, highlighted in green, are included in the model. b) SA scheme composed by four FF qubits where all inter-qubit interactions are included. c) STA scheme composed of four FF qubits where all inter-qubit interactions are included. The addition of a rotated replica of the STA leads to an hexagonal lattice as highlighted by the dashed gray lines.

the point at which the electron is shared halfway between the P donor and the interface, and of an AC electrical field E^i_{ac}. Both are used to manipulate the qubit. The interaction Hamiltonian $\hat{H}^{i,j}_{int}$ depends on the DC electrical field difference in qubit i and in qubit j, and it is proportional to r^{-3}_{ij}, where r_{ij} is the distance between the two qubits.[5,12]

In the 1D array model only the first neighbor inter-qubit interactions are included thus $\hat{H}^{i,j}_{int} = 0$ for $j > i + 1$, whereas in the other two 2D arrays all inter-qubit interactions are considered.

We simulate the case corresponding to $N = 4$, with the qubits arranged in a LA, in a SA and in a STA as depicted in **Figure 1**.

The STA can be described as a central qubit directly coupled with three equidistant qubits placed at the vertices of an equilateral triangle. The shortest inter-qubit distance r_0 is the same in all three arrays and is set to 360 nm.

The quantum gates under investigation here, namely the one-qubit gates $R_z(-\frac{\pi}{2})$ and $R_x(-\frac{\pi}{2})$ and the two-qubit gate $\sqrt{iSWAP}$, constitute a universal set of quantum gates achievable through total electrical manipulation,[5] applying the control sequences given by the $\Delta E_z(t)$ and $E_{ac}(t)$ signals reported in ref. [12].

In order to study the effect of multiple parallel operations, we apply simultaneously the one-qubit operations to two, three or four qubits in the array, and the two-qubit operations on four qubits. Each one of these cases, referred to as configurations, is labeled as reported in **Table 1**.

The figure of merit chosen to compare the different arrays is the entanglement fidelity F.[12,13] Following ref. [12] for each gate under study, one hundred instances of the charge noise with 1/f spectrum, ranging from $f_{min} = 50$ kHz to $f_{max} = 22$ GHz, are generated in the time domain with an amplitude $\alpha_{\Delta E_z}$ and added to the ideal sequence signals performing the operation for each qubit. Each qubit in the array is affected by a different noise instance because noise correlations between qubits are not considered. Finally, we take the average over the resulting entanglement infidelities.

Table 1. Correspondence between configurations and types of operation in the arrays.

Configuration	Type of Operation
ci ($i = 1, \ldots, N$)	One-qubit operation on qubit i while the others are idle
cij ($j \neq i = 1, \ldots, N$)	Two parallel one-qubit operations or single two-qubit operation on qubits i and j while the others are idle
cijk ($k \neq j \neq i = 1, \ldots, N$)	Three parallel one-qubit operations on qubits i, j and k while the other is idle
cijkl ($l \neq k \neq j \neq i = 1, \ldots, N$)	Four parallel one-qubit operations applied on all the qubits i, j, k and l
cij-kl ($l \neq k \neq j \neq i = 1, \ldots, N$)	Two parallel two-qubit operations on the qubit couples ij and kl

3. Results

In this Section, the results of simulated infidelities for parallel one-qubit and two-qubit operations are presented when the noise amplitude $\alpha_{\Delta E_z}$ spans a range from 0 to 100 V m^{-1}. For the one-qubit case, after presenting the outcome of a single operation (Section 3.1), the results of the infidelities for two, three, and four parallel operations are reported (Section 3.2). Then, simulation results for one two-qubit operation (Section 3.3) and two parallel two-qubit operations (Section 3.4) are shown.

3.1. One-Qubit Operations

Figure 2 shows the infidelity $1 - F$ as a function of the noise amplitude $\alpha_{\Delta E_z}$ when a one-qubit gate, $R_z(-\frac{\pi}{2})$ and $R_x(-\frac{\pi}{2})$, is performed on one qubit while the others are in an idle state a) in a LA, b) in a SA, and c) in a STA. The configurations of interest are the c1 and c2 configurations for the LA, the c1 for the SA and the c1 and c2 for the STA. All other possible configurations are geometrically equivalent to the ones presented and thus yield the same results for infidelities. This consideration holds from this point onward, regardless of the type of operations performed. All the gate infidelities increase as the noise amplitude is raised, with the infidelity of $R_x(-\frac{\pi}{2})$ being higher than that of $R_z(-\frac{\pi}{2})$.

In correspondence to a realistic noise amplitude, i.e., $\alpha_{\Delta E_z} = 50$ V m^{-1}, we report in **Table 2** the best and the worst infidelity values for each operation and for each array type, specifying in parenthesis the corresponding configuration.

The c1 configuration always shows the lower infidelity value in both $R_z(-\frac{\pi}{2})$ and $R_x(-\frac{\pi}{2})$ operations because it corresponds to a qubit that is less disturbed by the idle surrounding qubits. The LA is the most favorable geometry for performing single-qubit operations.

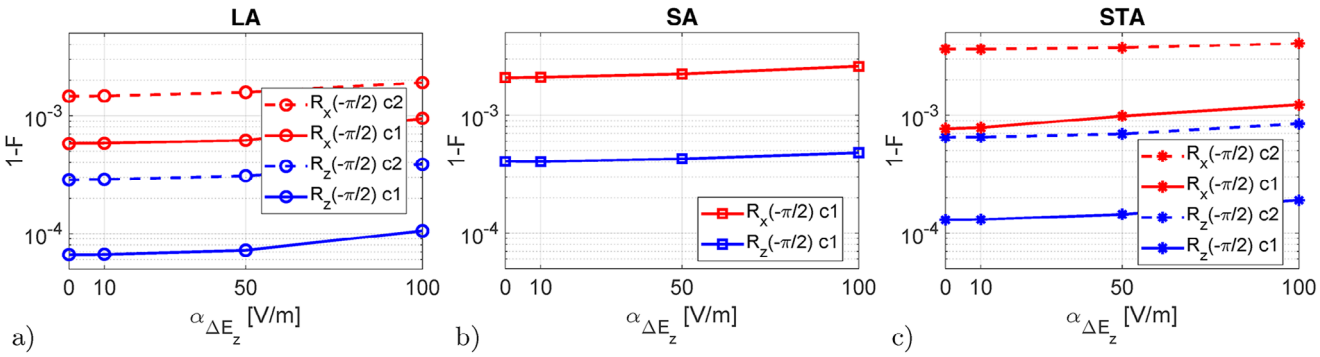

Figure 2. $R_z(-\frac{\pi}{2})$ (blue curves) and $R_x(-\frac{\pi}{2})$ (red curves) infidelities versus the noise amplitude $\alpha_{\Delta E_z}$ for a) the c1 and c2 configurations in the LA, b) the c1 configuration in the SA and c) the c1 and c2 configurations in the STA.

3.2. Parallel One-Qubit Operations

Figure 3a,b,c illustrates the infidelity $1-F$ as a function of the noise amplitude $\alpha_{\Delta E_z}$ when two parallel one-qubit gate, $R_z(-\frac{\pi}{2})$ and $R_x(-\frac{\pi}{2})$, are applied to a pair of qubits while the others are in an idle state. The analyzed configurations depend on the array geometry. Here, we study all pair of qubits at distances r_0 (configurations c12 and c23), $2r_0$ (configuration c13) and $3r_0$ (configuration c14) for the LA a). For the SA, we study pairs at distance r_0 and $\sqrt{2}r_0$ corresponding respectively to c12 and c13 b). In the STA, we consider pairs at distance r_0 and $\sqrt{3}r_0$, corresponding respectively to c12 and c13 c).

Figure 3d,e,f illustrates the infidelity $1-F$ as a function of the noise amplitude $\alpha_{\Delta E_z}$ when three parallel one-qubit gates, $R_z(-\frac{\pi}{2})$ and $R_x(-\frac{\pi}{2})$, are applied to a triplet of qubits while the fourth qubit remains idle. The analyzed configurations are c123 and c124 for LA d), c123 for SA e) and c123, c134 for STA f).

Figure 3g,h,i illustrates the infidelity $1-F$ as a function of the noise amplitude $\alpha_{\Delta E_z}$ for the three arrays when four parallel one-qubit gates, $R_z(-\frac{\pi}{2})$ and $R_x(-\frac{\pi}{2})$, are applied to all qubits.

We report in **Table 3** the best and the worst infidelity values for each operation and for each array type when $\alpha_{\Delta E_z} = 50$ V m^{-1} in correspondence to two, three and four parallel operations.

When two parallel one-qubit operations are performed, the number of possible configurations in the arrays studied increases, and we observed more variability in the infidelity values.

Table 2. One-qubit operations best an worst infidelity values when $\alpha_{\Delta E_z} = 50$ V m^{-1}, in parenthesis the corresponding configuration is specified.

Operation	$1-F_{LA}$	$1-F_{SA}$	$1-F_{STA}$
$R_z(-\frac{\pi}{2})$	7.2×10^{-5} (c1)	4.3×10^{-4} (c1)	1.4×10^{-4} (c1)
	3.1×10^{-4} (c2)	—	6.9×10^{-4} (c2)
$R_x(-\frac{\pi}{2})$	6.2×10^{-4} (c1)	2.2×10^{-3} (c1)	9.8×10^{-4} (c1)
	1.6×10^{-3} (c2)	—	3.7×10^{-3} (c2)

The LA allows for a larger number of configurations to be considered and the lowest infidelity values are obtained in the c14 configuration, where the operated qubits are at the extremes of the array. Conversely, higher infidelity values are found in the c13 and c23 configurations, although these configurations produce very similar results.

In the SA, the best infidelity values are obtained when the operated qubits are closer together (on the edge of the square) compared to configurations where they are farther apart (on the diagonal of the square). In the STA, it is preferable for the operated qubits to be on the edge of the triangle rather than having one qubit in the center, as the central qubit is much more affected by the disturbance from the idle qubits.

In general, we may conclude that the LA also provides better results for both one-qubit operations, even if the STA is preferred for the $R_x(-\frac{\pi}{2})$ operation.

The infidelity results when three parallel one-qubit operations are performed for the different configurations considered to yield similar outcomes in both the LA and the STA, while only one configuration for the SA is considered due to the symmetry of the array. For both operations, the SA shows larger infidelities compared to the STA and the LA. The LA configuration yields lower infidelity values for $R_z(-\frac{\pi}{2})$, while the STA configuration yields lower infidelity values for $R_x(-\frac{\pi}{2})$.

We observe that when four parallel one-qubit operations are performed for $R_z(-\frac{\pi}{2})$, the infidelity values are very close to the case in which three parallel one-qubit operations are performed, while for $R_x(-\frac{\pi}{2})$, the infidelities are larger. The LA is the preferred geometry for $R_z(-\frac{\pi}{2})$, while the SA gives a slightly better result for $R_x(-\frac{\pi}{2})$.

In summary, the LA is the geometry that gives the most promising results for the parallel $R_z(-\frac{\pi}{2})$ operations regardless of the number of performed operations. The $R_x(-\frac{\pi}{2})$ instead gives better infidelity results in the STA for two and three parallel operations, while the SA has to be preferred for four parallel operations.

3.3. Two-Qubit Operation

Moving from one-qubit gates to two-qubit gates, **Figure 4** shows the $1-F$ of the two-qubit operation $\sqrt{iSWAP}$ as a function of the

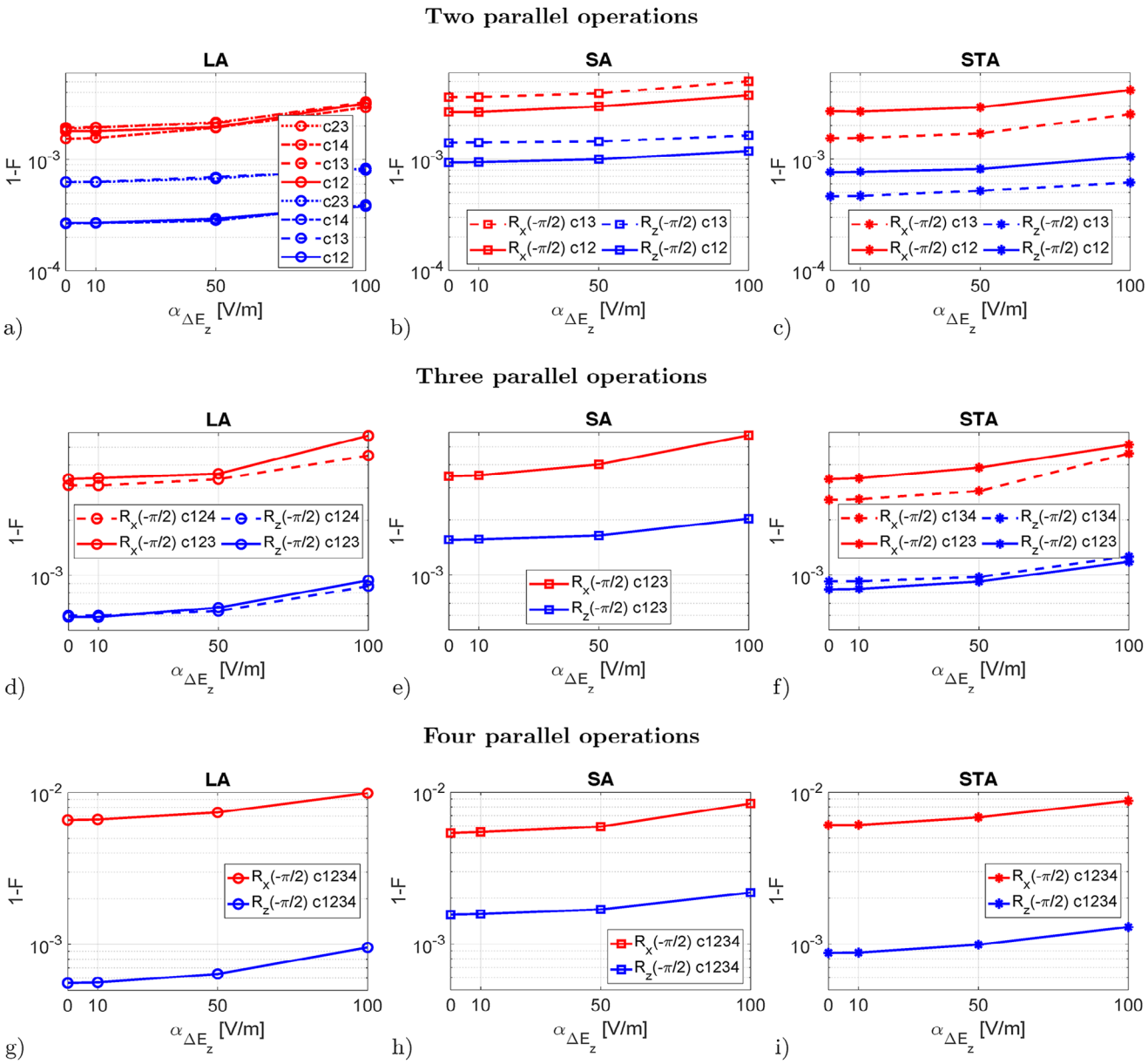

Figure 3. Two parallel $R_z(-\frac{\pi}{2})$ (blue curves) and $R_x(-\frac{\pi}{2})$ (red curves) infidelities versus the noise amplitude $\alpha_{\Delta E_z}$ for a) the c12, c13, c14 and c23 configurations in the LA, b) the c12 and c13 configurations in the SA and c) the c12 and c13 configurations in the STA. Three parallel $R_z(-\frac{\pi}{2})$ and $R_x(-\frac{\pi}{2})$ infidelities versus the noise amplitude $\alpha_{\Delta E_z}$ for d) the c123 and c124 configurations in the LA, e) the c123 in the SA and f) the c123 and c134 configurations in the STA. Four parallel $R_z(-\frac{\pi}{2})$ and $R_x(-\frac{\pi}{2})$ infidelities versus the noise amplitude $\alpha_{\Delta E_z}$ for the c1234 configuration in g) the LA, h) the SA and i) the STA.

noise amplitude $\alpha_{\Delta E_z}$, with the other two qubits in an idle state. This analysis is conducted for the c12 and c23 configurations in LA, the c12 configuration in SA and in STA. Only the configurations with an inter-qubit distance equal to r_0 are considered for the $\sqrt{iSWAP}$ gate. As expected, the infidelities of the $\sqrt{iSWAP}$ gate increase as the noise amplitude is incremented, with the different curves assuming closer values as $\alpha_{\Delta E_z}$ increases.

The infidelities of the $\sqrt{iSWAP}$ at $\alpha_{\Delta E_z} = 50\ \mathrm{V\,m^{-1}}$ are reported in **Table 4**.

The LA is the only array that allows two different configurations, with the lowest value corresponding to c23. The SA provides the best result at this $\alpha_{\Delta E_z}$ value.

3.4. Parallel Two-Qubit Operations

Figure 5 displays the $1 - F$ of two parallel $\sqrt{iSWAP}$ gates compared to the noise amplitude $\alpha_{\Delta E_z}$ for the c12-34 configuration in the LA and in the SA. No results are provided for the STA because

Table 3. Best and worst infidelity values for each operation and for each array type when $\alpha_{\Delta E_z}$ =50 V m^{-1} in correspondence to two, three and four parallel operations, in parenthesis the corresponding configuration is specified.

Number of parallel operations	Operation	$1-F_{LA}$	$1-F_{SA}$	$1-F_{STA}$
2	$R_z(-\frac{\pi}{2})$	2.8×10^{-4} (c14)	1.0×10^{-3} (c12)	5.2×10^{-4} (c13)
		6.9×10^{-4} (c13)	1.4×10^{-3} (c13)	8.2×10^{-4} (c12)
	$R_x(-\frac{\pi}{2})$	1.9×10^{-3} (c14)	3.0×10^{-3} (c12)	1.7×10^{-3} (c13)
		2.2×10^{-3} (c23)	3.9×10^{-3} (c13)	2.9×10^{-3} (c12)
3	$R_z(-\frac{\pi}{2})$	6.4×10^{-4} (c124)	1.6×10^{-3} (c123)	9.2×10^{-4} (c123)
		6.6×10^{-4} (c123)	—	9.7×10^{-4} (c134)
	$R_x(-\frac{\pi}{2})$	3.3×10^{-3} (c124)	4.0×10^{-3} (c123)	2.9×10^{-3} (c134)
		3.6×10^{-3} (c123)	—	3.9×10^{-3} (c123)
4	$R_z(-\frac{\pi}{2})$	6.4×10^{-4} (c1234)	1.7×10^{-3} (c1234)	9.9×10^{-4} (c1234)
	$R_x(-\frac{\pi}{2})$	7.4×10^{-3} (c1234)	5.9×10^{-3} (c1234)	6.8×10^{-3} (c1234)

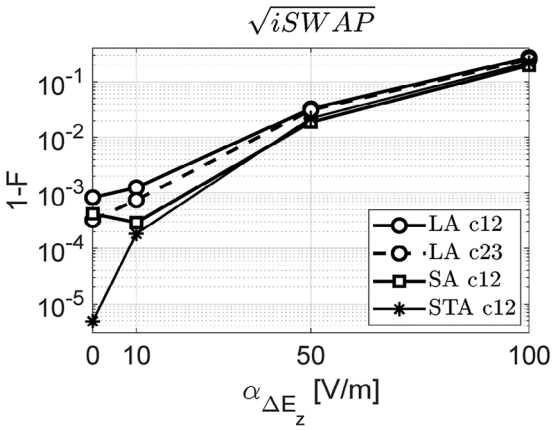

Figure 4. $\sqrt{iSWAP}$ infidelity as a function of the noise amplitude $\alpha_{\Delta E_z}$ for the c12 and c23 configurations in the LA (circles), the c12 configuration in the SA (squares) and the c12 configuration in the STA (stars).

Table 4. $\sqrt{iSWAP}$ infidelity values when $\alpha_{\Delta E_z}$ = 50 V m^{-1}, in parenthesis the corresponding configuration is specified.

Operation	$1-F_{LA}$	$1-F_{SA}$	$1-F_{STA}$
$\sqrt{iSWAP}$	3.1×10^{-2} (c23)	1.9×10^{-2} (c12)	2.2×10^{-2} (c12)

in this array it is not feasible to apply two parallel two-qubit operations with an inter-qubit distance equal to r_0. As the noise amplitude increases, the infidelities of two parallel $\sqrt{iSWAP}$ gates also increase. Specifically, the LA exhibits lower infidelity compared to the SA configuration.

The resulting infidelity values when $\alpha_{\Delta E_z}$ is set to 50 V m^{-1} are reported in **Table 5**.

Table 5. $\sqrt{iSWAP}$ infidelity values when $\alpha_{\Delta E_z}$ = 50 V m^{-1}, in parenthesis the corresponding configuration is specified.

Number of parallel operations	Operation	$1-F_{LA}$	$1-F_{SA}$
2	$\sqrt{iSWAP}$	1.9×10^{-1} (c12-34)	2.3×10^{-1} (c12-34)

We observe high infidelity values in both cases, but the LA performs better than the SA.

4. Discussion

In **Figure 6**, the simulated infidelity of each considered gate applied to all the configuration in the three different arrays is reported as a function of the number of applied parallel operations.

Figure 6a displays the infidelity results of $R_z(-\frac{\pi}{2})$, demonstrating significant variability between different configurations in different arrays for one and two parallel operations. Moreover, the infidelity saturates as the number of parallel operations exceeds two, regardless of the array type.

For each array, the plateau is effectively highlighted by the dashed line passing through points obtained by averaging the infidelities over different configurations with the same number of parallel operations. Figure 6a shows that the average infidelity in LA (1-F = 6.4×10^{-4}) is lower than that in STA (1-F = 9.9×10^{-4}), which in turn is lower than that in SA (1-F = 1.7×10^{-3}). This ordering of infidelity plateaus corresponds to the one provided by

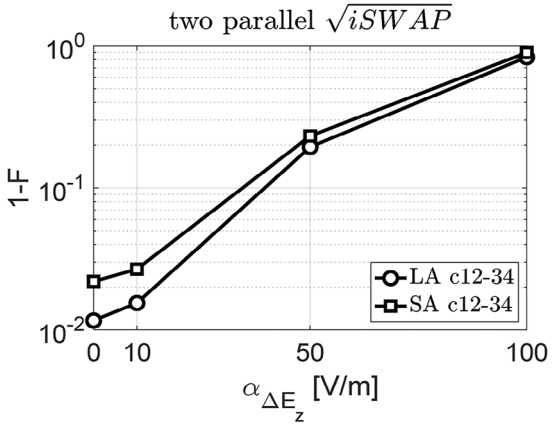

Figure 5. Two parallel $\sqrt{iSWAP}$ infidelities as a function of the noise amplitude $\alpha_{\Delta E_z}$ for the LA (circles) and the SA (squares) in the c12-34 configuration.

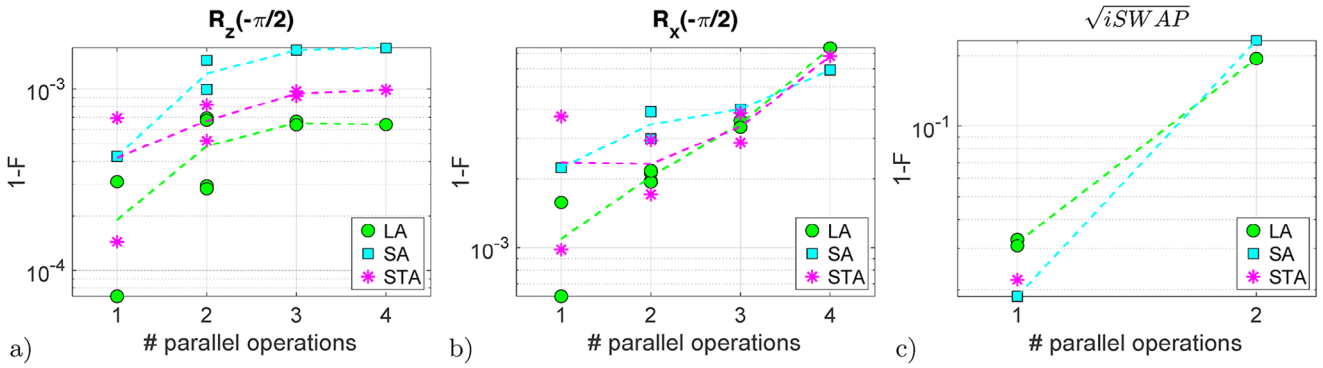

Figure 6. Infidelity of all configurations in the LA (green circles), SA (cyan squares) and STA (magenta stars) as a function of the number of parallel a) $R_z(-\frac{\pi}{2})$ b) $R_x(-\frac{\pi}{2})$ and c) $\sqrt{iSWAP}$ gate(s) when $\alpha_{\Delta E_z} = 50$ V m^{-1}. The dashed lines connect points representing the average infidelity values over different configurations for each number of parallel operations.

analyzing the parameter δ in the three different arrays, that gives an estimation of the interaction density and is defined here as:

$$\delta \equiv \sum_{i=1}^{N-1} \sum_{j=2, j>i}^{N} f(r_{ij}) \tag{2}$$

where $f(r_{ij})$ is a function of the inter-qubit distance r_{ij} between qubit i and qubit j. Given that each array of FF qubits has an interacting Hamiltonian $\hat{H}_{int}$ proportional to r_{ij}^{-3} (see Equation 6 in ref. [12]) it is natural to choose $f(r_{ij}) = r_{ij}^{-3}$. The resulting δ values for the three arrays considered are $\delta_{LA} = 3.29\ r_0^{-3}$, $\delta_{STA} = 3.51\ r_0^{-3}$, and $\delta_{SA} = 4.70\ r_0^{-3}$. Thus $\delta_{LA} < \delta_{STA} < \delta_{SA}$.

In Figure 6b, the infidelity of $R_x(-\frac{\pi}{2})$ similarly exhibits significant variability among different configurations in different arrays for a single operation, while the variability decreases as the number of parallel operation increases. The average infidelity strongly increases with the number of parallel gates. These increasing trends can be qualitatively explained by considering that the addition of parallel control signals, which modulate the energy of each qubit, also modifies the Electric Dipole Spin Resonance (EDSR) frequency of each qubit due to unwanted qubit mutual coupling. Since the AC control signal frequency applied to each qubit in the array is set to a constant value corresponding to the EDSR frequency of an isolated FF qubit, the qubits are progressively driven further out of resonance as the number of parallel operations applied to the array increases. This causes an infidelity increase of the entire operation which, however, does not exceed 8×10^{-3} for four parallel operations.

It is worth pointing out that in Figure 6a,b, the STA configurations with the highest infidelities - namely c2, c12, c123, and c1234 for increasing number of parallel operations - include the central qubit, denoted by Index 2. The central qubit has the highest interaction with the other three noisy qubits, being distant r_0 from each one of the three qubits, a condition not met by the other qubits in STA. This unwanted coupling effect on the central qubit is particularly evident when focusing on a single operation, where the STA configuration c2 yields the worst results among the different arrays.

In Figure 6c the infidelity of $\sqrt{iSWAP}$ shows less significant variability between different configurations in different arrays for both one and two parallel two-qubit operations than one-qubit gate infidelities. The average $\sqrt{iSWAP}$ infidelities increase as the number of parallel gates is increased, ranging from 0.02 for one operation to 0.2 for two parallel ones. This confirms that two-qubit gates are likely to be the limiting factor for the successful execution of an algorithm and poses a roadblock in the exploitation of parallel two-qubit gating in such small arrays of FF qubits.

The results shown only apply to arrays of four FF qubits, and accurate assessments of the error of parallel gates in larger arrays can only be achieved by running more complex simulations with many qubits. However, a qualitative discussion regarding the potential extensibility of considerations for LA, SA, and STA to large-scale arrays can be made. In particular, for large linear arrays, the same qualitative relationship between one-qubit gate infidelities on edge and inner LA qubits is expected to hold, with smaller 1-F values on edge qubits compared to inner ones. This consideration, however, cannot be directly extended to large square arrays, as the SA with only four qubits consists solely of edge qubits, thus not capturing the effects of inner qubits present in larger square arrays. Conversely, according to the STA findings, it seems reasonable to expect a similar relationship between 1-F values for one-qubit gates applied to the central qubit and edge ones even in large hexagonal arrays, with inner qubits likely performing worse than edge qubits. When parallel gating in large-scale arrays is considered, it is reasonable to expect behaviors not dissimilar to those reported in Figure 6, potentially resulting in increased infidelities due to more qubits interacting undesirably.

5. Conclusion

The effects of parallel gating on the entanglement gate fidelity have been simulated in LA, SA and STA of four FF qubits affected by 1/f noise.

Upon comparing the fidelity results among the three arrays at a reasonable noise level, we observed a lower average $R_z(-\pi/2)$ infidelity in the LA compared to the SA and STA. The infidelity values saturate as the number of parallel operations exceeds two. For $R_x(-\pi/2)$, the infidelities are higher than those for $R_z(-\pi/2)$, but the differences in average infidelities among the arrays decreases as the parallelism of $R_x(-\pi/2)$ increases. A similar trend

is observed for $\sqrt{iSWAP}$ gates, which exhibit the highest infidelities. Parallel $\sqrt{iSWAP}$ gates result in very high infidelities suggesting that parallelization of two-qubit operations should be avoided in such small arrays.

The infidelity results of each gate in each configuration versus the number of parallel operations reported in this study provide critical information for a quantum compiler. This information helps in selecting the optimal quantum circuit, including the correct sequence of gates with the best depth and parallelism, to implement the desired quantum algorithm with the lowest infidelity.

Acknowledgements

The work was partially funded by PNRR MUR projects PE0000023-NQSTI and CN0000013-HPC financed by the European Union – Next Generation EU.

Open access publishing facilitated by Consiglio Nazionale delle Ricerche, as part of the Wiley - CRUI-CARE agreement.

Conflict of Interest

The authors declare no conflict of interest.

Data Availability Statement

The data that support the findings of this study are available from the corresponding author upon reasonable request.

Keywords

flip-flop qubit, parallel gating, qubit arrays, silicon qubit

Received: July 19, 2024
Revised: September 6, 2024
Published online:

[1] L. M. K. Vandersypen, H. Bluhm, J. S. Clarke, A. S. Dzurak, R. Ishihara, A. Morello, D. J. Reilly, L. R. Schreiber, M. Veldhorst, *npj Quantum Inf.* **2017**, *3*, 34.
[2] J. C. McCallum, B. C. Johnson, T. Botzem, *Appl. Phys. Rev.* **2021**, *8*, 031314.
[3] G. Burkard, T. D. Ladd, A. Pan, J. M. Nichol, J. R. Petta, *Rev. Mod. Phys.* **2023**, *95*, 025003.
[4] M. De Michielis, E. Ferraro, E. Prati, L. Hutin, B. Bertrand, E. Charbon, D. J. Ibberson, M. F. Gonzalez-Zalba, *J. Phys. D: Appl. Phys.* **2023**, *56*, 363001.
[5] G. Tosi, F. A. Mohiyaddin, V. Schmitt, S. Tenberg, R. Rahman, G. Klimeck, A. Morello, *Nat. Commun.* **2017**, *8*, 450.
[6] G. Tosi, F. A. Mohiyaddin, S. Tenberg, A. Laucht, A. Morello, *Phys. Rev. B* **2018**, *98*, 075313.
[7] A. Morello, J. J. Pla, P. Bertet, D. N. Jamieson, *Adv. Quantum Technol.* **2020**, *3*, 2000005.
[8] E. Ferraro, D. Rei, M. Paris, M. De Michielis, *EPJ Quantum Technol.* **2022**, *9*, 2.
[9] D. Rei, E. Ferraro, M. De Michielis, *Adv. Quantum Technol.* **2022**, *5*, 2100133.
[10] F. A. Calderon-Vargas, E. Barnes, S. E. Economou, *Phys. Rev. B* **2022**, *106*, 165302.
[11] R. Savytskyy, T. Botzem, I. F. de Fuentes, B. Joecker, J. J. Pla, F. E. Hudson, K. M. Itoh, A. M. Jakob, B. C. Johnson, D. N. Jamieson, A. S. Dzurak, A. Morello, *Sci. Adv.* **2023**, *9*, eadd9408.
[12] M. De Michielis, D. Rei, E. Ferraro, *Adv. Quantum Technol.* **2024**, *7*, 2300455.
[13] M. A. Nielsen, *arXiv:quant-ph/9606012* **1996**.